

Antiferromagnetic-to-ferromagnetic Transition in the $\text{GdNiSi}_{1-x}\text{Al}_x$ Compound

R. D. Mukhachev¹⁾, A. V. Lukoyanov^{1)*}, A. G. Kuchin^{1)†}

[†]M. N. Mikheev Institute of Metal Physics of Ural Branch of Russian Academy of Sciences, 620108 Ekaterinburg, Russia

^{*}Institute of Physics and Technology,

Ural Federal University named after the first President of Russia B. N. Yeltsin, 620002 Ekaterinburg, Russia

Submitted 11 March 2024

Resubmitted 15 April 2024

Accepted 18 April 2024

In this work, the electronic structure and magnetic properties of GdNiSi have been investigated within the framework of theoretical DFT + U method. The antiferromagnetic ordering of the Gd moments was obtained as the ground state, whereas Ni and Si have negligible magnetic moments. An antiferromagnetic-to-ferromagnetic transition was found when GdNiSi is doped with Al in our theoretical calculations. The antiferromagnetic-to-ferromagnetic transition takes place in the Gd sublattice, the magnetic moments at the Gd ions remain the same but the type of magnetic ordering changes. It was found that even at concentrations as low as $x = 0.1$, the ferromagnetic ordering in the Gd sublattice is more favorable in total energy as the ground state which can be ascribed to the shortening of Gd-Gd distances and the oscillating behavior of the Ruderman-Kittel-Kasuya-Yosida interaction in the Al-doped compositions. The electronic structure demonstrates significant changes in the vicinity of the localized Gd $4f$ states that confirms the presence of the antiferromagnetic-to-ferromagnetic transition using our theoretical results for Al $x \geq 0.1$ in good agreement with the previous experimental magnetic results.

DOI: 10.1134/S0021364024600757

In recent years, interest in ternary intermetallics RTX based on rare earth metals has increased significantly. RTX compounds are composed of R – a rare-earth metal and T, X – different d or p -elements [1]. This is due to the presence of many interesting properties, such as: giant and large magnetocaloric effect (MCE) and magnetoresistance (MR), metamagnetic transitions, magneto-structural coupling, spin glass state, heavy fermion behavior, superconductivity [2–4]. This is accompanied by the structural diversity of this group [5, 6]. There are many RTX compounds with magnetic ordering temperatures above room temperature and reaching 510 K [2]. One of the interesting and well-studied compounds of this class is HoNiAl . This ternary compound was found to have two phase transitions [7], the doping of HoNiAl with copper is also interesting. $\text{HoNi}_{0.9}\text{Cu}_{0.1}\text{Al}$ shows two phase transitions near 5.7 and 11.8 K, which are explained by the coexistence of ferromagnetic (FM) and antiferromagnetic (AFM) ordering components, and shows a “table-like” change in magnetic entropy with small field changes, with a large refrigerant capacity and without loss of hysteresis [8]. And when the copper concentration is greater than 0.8,

the magnetic ordering changes from AFM to FM with a possible cause being the AFM magnetic component re-orientation [9]. In ErNiSi , a high value of magnetocaloric effect and MR were found at temperatures up to 20 K [10, 11]. HoNiSi undergoes an AFM-FM transition under the influence of magnetic field, and displays a giant reversible magnetocaloric effect at a relatively low field [12, 13]. An AFM – paramagnetic (PM) transition was observed in HoNiGa near Néel temperature 10 K or under the influence of a field and with large MCE and perfect reversibility [14].

Among other ternary RTX compounds, gadolinium-based compounds GdTX are of particular interest not only due to the magnetocaloric properties characteristic of this group, but also due to the variety of possible structures and magnetic properties [15, 16]. Experimentally and theoretically, it was found that doping most GdTX compounds can improve their magnetic and other properties [1, 17]. Thus, Curie temperature can vary in a wide range from 20 to 98 K in the $\text{Gd}_{1-x}\text{Ho}_x\text{NiIn}$ compounds, and also achieve high refrigerant capacity (RC) with the highest value of 443 J/kg [18]. This compound also exhibits a para-FM phase transition at low temperatures 5 and 20 K. In addition to the transitions caused by temperature

¹⁾e-mail: r.d.mukhachev@imp.uran.ru

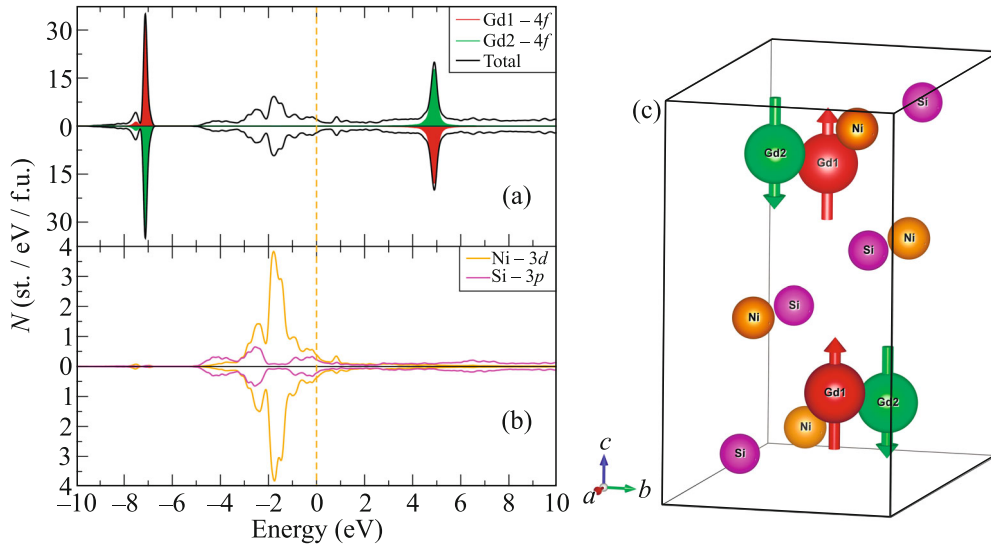


Fig. 1. (Color online) Total (a) and partial (b) densities of electronic states of GdNiSi; the crystal structure (c) of GdNiSi with the AFM ordering. Gd1 atoms are shown in red, Gd2 in green, Ni in orange, Si in magenta

or external field, there are also those that depend on changes in composition. It was recently discovered in $\text{GdFe}_{1-x}\text{Ni}_x\text{Si}$ [19] that for $x \geq 0.3$, an AFM ordering becomes energetically preferable rather than FM, as at the lower concentrations of Ni and in pure GdFeSi . Another composition-induced magnetic transition was proposed in $\text{GdMn}_{1-x}\text{Ti}_x\text{Si}$ for $x = 0-1$ [20]. Recently, the Al-doped $\text{GdNiSi}_{1-x}\text{Al}_x$ system was first synthesized and experimentally studied in order to improve its magnetocaloric properties, it was found to almost double the values of the relative cooling power for $x = 0.2$ [21]. It was reported that an increase in the aluminum concentration leads to a transition from an AFM to FM ordering because GdNiAl possesses a hexagonal ZrNiAl -type structure and FM ground state [21]. No such magnetic transitions were found in, e.g. $\text{GdFeAl}_{1-x}\text{Si}_x$ [16]. Some RNiSi compounds are reported to have giant or large MCE [2, 10, 12, 13], then doping with p elements might be a mechanism for boosting MCE to the higher values. In our work, we performed theoretical calculations of the electronic structure and magnetic properties for the modelled $\text{GdNiSi}_{1-x}\text{Al}_x$ compositions for $x = 0-0.3$ to advance understanding of the electronic structure and changes of the magnetic orderings.

The electronic structure, magnetic moments and types of magnetic orderings were investigated using the DFT + U method in Quantum ESPRESSO package [22, 23] for exchange-correlation functional as generalized gradient approximation (GGA-PBE) [24]. For convergence, 60 Ry was taken as an energy cutoff for plane waves. A grid of $12 \times 12 \times 12$ k -points was set in reciprocal space. Projected augmented wave dataset

for Gd [25] and standard PAW pseudo-potentials of the other elements were chosen from library of Quantum ESPRESSO [26]. Strong electron correlations in the Gd 4*f* shell were taken into account in the GGA + U approach for the Coulomb parameter as 6.7 eV and Hund parameter as 0.7 eV, the same values as usually used in different Gd non-oxide compounds [1, 3, 19, 20]. Structural data for our calculations were taken from [21], which are close to GdNiSi from [27], for a supercell of GdNiSi with 4 formula units. GdNiSi crystallizes into orthorhombic structure $Pnma$, space group (SG) # 62 [21], this structure was also used for our calculations of the Al-doped compounds.

Our calculations were made for the experimental crystal structure parameters for three Al concentrations of 10, 20 and 30 % [21]. However, the supercell with 12 atoms, i.e., nominal 25 % was modelled for the experimental crystal structure parameters of all compositions. Table 1 shows the crystal structure parameters, cell volumes and the distances between atoms, both the nearest neighbors and the next nearest neighbors, based on structural data for all compounds under consideration. Also, experimental atomic coordinates from [21] for different Al concentrations of 10, 20 and 30 % were used in our calculations, not shown in Table 1. It can be seen that the cell volume decreases with the addition of aluminum, except for an increase in $\text{GdNiSi}_{0.7}\text{Al}_{0.3}$ is most likely due to the presence of another impurity phase that is strongly manifested in the higher Al content alloys [21], therefore these results may not correspond to the general trend. The distances between the nearest gadolinium atoms gradually decrease when

Table 1. Crystal structure parameters in Å, cell volume in Å³ and interatomic distances d in Å for the $\text{GdNiSi}_{1-x}\text{Al}_x$ ($x = 0-0.3$) compositions for the structural data [21]

Composition/Characteristics	GdNiSi	GdNiSi _{0.9} Al _{0.1}	GdNiSi _{0.8} Al _{0.2}	GdNiSi _{0.7} Al _{0.3}
a , Å	6.9934	6.9682	6.9512	7.0267
b , Å	4.1809	4.2030	4.2068	4.2695
c , Å	7.2224	7.1968	7.1890	7.2894
Cell volume, Å ³	211.1739	210.7755	210.2233	218.6859
$d(\text{Gd1-Gd2})_{NN}$, Å	3.57	3.56	3.53	3.59
$d(\text{Gd2-Gd2})_{NNN}$, Å	4.82	4.79	4.72	4.89
$d(\text{Gd1-Gd2})_{NNN}$, Å	5.44	5.42	5.37	5.41
$d(\text{Gd1-Gd1})_{NNN}$, Å	7.84	7.81	7.77	7.78
$d(\text{Ni-Ni})_{NN}$, Å	4.30	4.31	4.26	4.24
$d(\text{Si-Si})_{NN}$, Å	4.08	4.07	4.13	4.14

modeling an increase in the concentration of aluminum in the system.

The densities of states N for GdNiSi are plotted in Fig. 1a, b for two spin projections (majority and minority). The Fermi energy is drawn as a vertical dashed orange line at zero energy (Fig. 1a, b). The total DOS and the $4f$ states of two types of the Gd ions forming the AFM ordering in GdNiSi are in Fig. 1a. These states indicated as Gd1 in red and Gd2 in green and their most intense peaks are in the energy ranges from -8 to -7 eV in the valence band and from 4.5 to 5.5 eV in the conduction band, symmetrically for both spin projections. Below the Fermi level, from -3 to 0 eV, there are highly intense, symmetrical peaks of the $3d$ states of nickel, indicated in orange. The contribution to the Fermi-level states is almost equally distributed between the $3d$ states of nickel and the $3p$ states of silicon. The crystal structure of GdNiSi in a supercell comprising 12 atoms, which was used for our calculations, is presented in Fig. 1c with the same colors as in Fig. 1a, b. The crystal structure is represented by an orthorhombic structure of the TiNiSi -type SG # 62. This figure clearly shows the relative arrangement of the antiferromagnetically ordered gadolinium atoms.

The electronic structure of $\text{GdNiSi}_{1-x}\text{Al}_x$ for $x = 0.25$ is plotted in Fig. 2. In comparison with the pure GdNiSi (Fig. 1), it has only 2 pronounced highly polarized peaks of gadolinium (red) states in Fig. 2a due to the Gd FM ordering and one type of the Gd ions. The gadolinium peaks are located in the same energy ranges as in Fig. 1a, but they are present in different spin projections for the occupied and empty $4f$ states. Figure 2b shows the states of nickel and p elements. As in GdNiSi , the nickel $3d$ states are represented by almost symmetrical peaks below the Fermi level. The $3p$ states of silicon and aluminum have low intensity peaks and are represented by a widely distributed band of states from -5 eV and above.

Also, in Fig. 2b one can see a slight decrease in the intensity of nickel states associated with the appearance of aluminum in the composition. The states of aluminum themselves are represented by the lowest intensity among all in this figure, almost evenly distributed over the entire energy range. To take doping into account, one silicon atom was replaced by aluminum in all compounds, as shown in Fig. 2c of the crystal structure parameters of $\text{GdNiSi}_{0.7}\text{Al}_{0.3}$. Also, from this figure one can see the similarity of all gadolinium atoms and the absence of AFM ordering, respectively.

In our self-consistent DFT + U calculations, the theoretical total magnetic moment of $\text{GdNiSi}_{1-x}\text{Al}_x$ was found to be solely formed by the Gd ion, and Ni, Si, Al are either non-magnetic or have very small magnetic moments, see Table 2. Changing the doping parameters has little effect on the magnetic moments, and the total magnetic moment of all FM compounds does not change. The DFT + U calculations confirmed that the pure intermetallic GdNiSi compound has an AFM state in the Gd sublattice as its ground state. The ordering of the Gd moments being aligned antiferromagnetically oriented between nearby atoms, which corresponds to G-type AFM. This type of AFM is more stable in GdNiSi than the ferromagnetic one with the differences in total energy equal to 1.03 meV/f.u., see Table 2. For the total energy differences, the estimated self-consistent accuracy ΔE_{acc} , which is provided in Quantum Espresso program for each total energy value as an estimate of the total energy error and is modified to account for magnetic calculations and U correction, was included in Table 2.

Doping of GdNiSi even with small amounts of Al dramatically changes the magnetic ordering type. It was found that, starting with the modelled $\text{GdNiSi}_{0.9}\text{Al}_{0.1}$ compound, the most energy-favorable ordering in the Gd sublattice becomes FM. We checked different types of the AFM orderings of the Gd moments. Data on

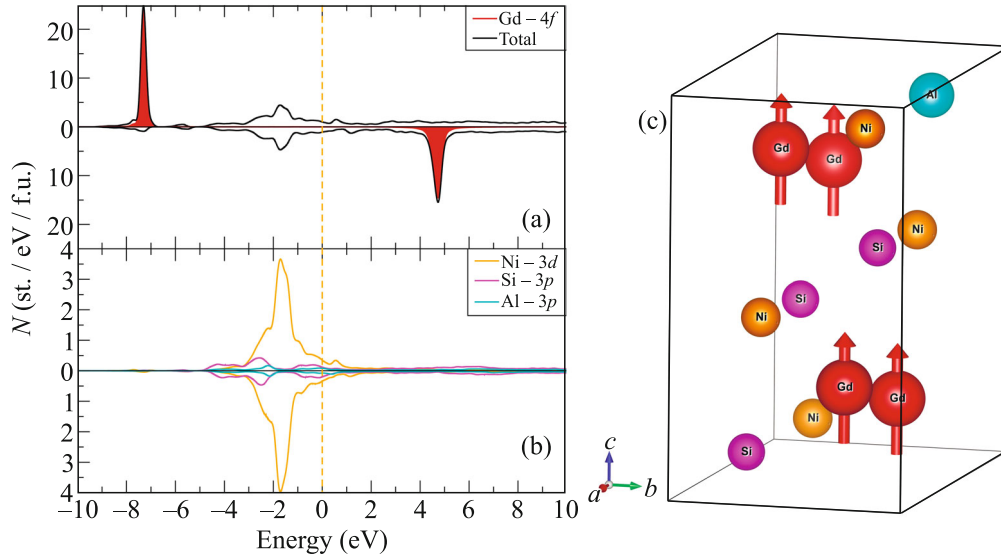


Fig. 2. (Color online) Total (a) and partial (b) densities of electronic states of modelled $\text{GdNiSi}_{0.75}\text{Al}_{0.25}$; the crystal structure (c) of $\text{GdNiSi}_{0.75}\text{Al}_{0.25}$ with the FM ordering. Gd atoms are shown in red, Ni in orange, Si in magenta, Al in cyan

Table 2. Total energy difference $\Delta E = |E_{\text{FM}} - E_{\text{AFM}}|$ in meV/f.u. relative to the lowest type of magnetic ordering of the Gd moments, estimated self-consistent accuracy ΔE_{acc} of ΔE , total and partial magnetic moments M for the modelled $\text{GdNiSi}_{1-x}\text{Al}_x$ ($x = 0-0.3$) compositions

Composition/Characteristics	GdNiSi	GdNiSi _{0.9} Al _{0.1}	GdNiSi _{0.8} Al _{0.2}	GdNiSi _{0.7} Al _{0.3}
ΔE (AFM), meV/f.u.	0	3.26	4.02	2.32
ΔE (FM), meV/f.u.	1.03	0	0	0
ΔE_{acc} , meV/f.u.	0.003	0.002	0.003	0.002
$M_{\text{Gd1/Gd2}}$, μ_B	-7.07/7.07	7.07	7.07	7.08
$M_{\text{Ni1/Ni2}}$, μ_B	-0.01/0.01	-0.03	-0.03	-0.04
$M_{\text{Si/Al}}$, μ_B	0	-0.01/0.02	-0.01/0.02	-0.01/0.02
M_{Total} , μ_B	0	7.03	7.03	7.03

the differences in energy between the FM and G-type AFM states, which was the most favorable among all other types, as well as lattice volumes for all studied compounds are presented in Table 2 and 1. The ferromagnetic state remains the most stable in total energy in all modelled Al-doped compounds, see Table 2 and Fig. 3. The energy difference in these cases ranges from 2.32 ($\text{GdNiSi}_{0.7}\text{Al}_{0.3}$) to 4.02 ($\text{GdNiSi}_{0.8}\text{Al}_{0.2}$) meV/f.u. From Figure 3, one can estimate the transition point for the Al concentration x equal to 0.024, i.e. 2.4% Al, which is very close to $x = 0$. All calculated energy differences are above the estimated self-consistent accuracy in the calculations, see Table 2. Such energy differences are characteristic for the Gd intermetallic compounds, e.g., for GdFeSi , the FM-AFM energy difference was calculated as 43 K (3.7 meV) in [28] or 7.9 meV [29]. Nevertheless, for gadolinium metal this energy difference was calculated as high as 30.935 meV/Gd [30] that is expected for the stable FM ordering.

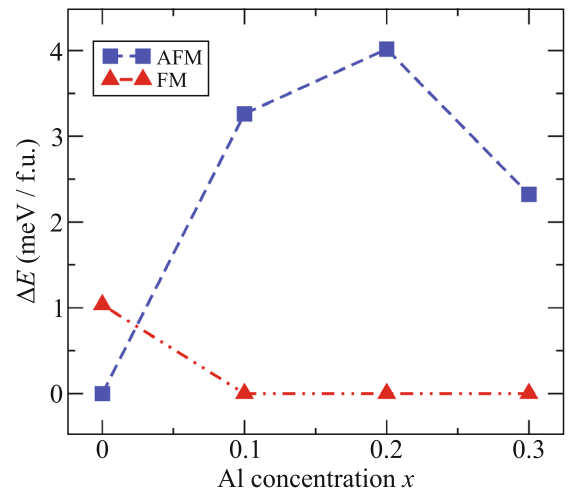


Fig. 3. (Color online) Total energy difference ΔE from Table 2 relative to the Al composition $x = 0, 0.1, 0.2, 0.3$ for $\text{GdNiSi}_{1-x}\text{Al}_x$

As a result of replacing a small part of silicon atoms with aluminum, see Table 1, there is a decrease in the distances between Gd atoms and the lattice volume as a whole. The decrease of the Gd-Gd distance can be clearly traced for the next-nearest neighbors $d(\text{Gd1-Gd2})_{NNN}$ and $d(\text{Gd1-Gd1})_{NNN}$ for all $x = 0-0.3$ structural data. However, for the nearest neighbors $d(\text{Gd1-Gd2})_{NN}$ and the next-nearest neighbors $d(\text{Gd2-Gd2})_{NNN}$ are decreasing for $x = 0-0.2$, then grows for $x = 0.3$ which we discuss below. The changes of the Gd-Gd distances are accompanied by with exchange coupling changes. As it is well known, the Ruderman-Kittel-Kasuya-Yosida (RKKY) interaction oscillates with the distance [31] and dominates the exchange coupling between the Gd-Gd ions [32, 33]. Then it can govern a transition from AFM to FM ordering for the Al-doped compounds, but the presence of Al is also significant for the FM formation, as at $x = 0.3$, the FM ordering is preserved despite the increase of some Gd-Gd distances. The short Gd-Gd distances were previously found in the other FM Gd-based ternary compounds, for example, in GdRuSi [20]. Also, from Table 1, one can see that in the $\text{GdNiSi}_{0.7}\text{Al}_{0.3}$ composition the lattice volume increases by 3.7% compared to GdNiSi . This result might be caused by an impurity phase, which is supported by a rapid cell volume increase and affected the results of experimental measurements for the higher Al content [21] but require additional experimental studies including neutron diffraction.

Thus, in our work, the magnetic properties and electronic structure of $\text{GdNiSi}_{1-x}\text{Al}_x$ were modeled theoretically for the experimental crystal structure parameters for the Al content equal to 10, 20 and 30%. In the calculations, strong electron correlations of Gd $4f$ were taken into account within GGA + U . The AFM-FM transition was estimated for the Al-concentration as low as $x = 0.024$ within the range $x = 0-0.1$. It occurs in the Gd sublattice with the same values of Gd moments in good agreement with the previous experimental magnetic results. The AFM ordering in GdNiSi is more energetically favorable, while in $\text{GdNiSi}_{1-x}\text{Al}_x$ the FM ordering is found as the ground state which can be due to the presence of Al and shortening of the Gd-Gd distances. The localized Gd $4f$ electronic states are also modified in the AFM-FM transition for Al $x \geq 0.1$. The concentration-driven magnetic transition is promising for the Gd-based compounds and will motivate further research. Therefore, further study of their properties may be useful for various environmentally sustainable applications.

Funding. This study was supported by the grant of Russian Science Foundation # 24-22-00066,

<https://rscf.ru/en/project/24-22-00066/>, M.N. Mikheev Institute of Metal Physics of Ural Branch of Russian Academy of Sciences.

Conflict of interest. The authors of this work declare that they have no conflicts of interest.

Open Access. This article is licensed under a Creative Commons Attribution 4.0 International License, which permits use, sharing, adaptation, distribution and reproduction in any medium or format, as long as you give appropriate credit to the original author(s) and the source, provide a link to the Creative Commons license, and indicate if changes were made. The images or other third party material in this article are included in the article's Creative Commons license, unless indicated otherwise in a credit line to the material. If material is not included in the article's Creative Commons license and your intended use is not permitted by statutory regulation or exceeds the permitted use, you will need to obtain permission directly from the copyright holder. To view a copy of this license, visit <http://creativecommons.org/licenses/by/4.0/>.

1. A. G. Kuchin, S. P. Platonov, A. V. Lukoyanov, A. S. Volegov, V. S. Gaviko, R. D. Mukhachev, and M. Yu. Yakovleva, *Intermetallics* **133**, 107183 (2021).
2. H. Zhang, Y. W. Li, E. Liu, Y. J. Ke, J. L. Jin, Y. Long, and B. G. Shen, *Sci. Rep.* **5**, 11929 (2015).
3. A. G. Kuchin, S. P. Platonov, R. D. Mukhachev, A. V. Lukoyanov, A. S. Volegov, V. S. Gaviko, and M. Yu. Yakovleva, *Metals* **13**, 290 (2023).
4. H. Zhang and B. G. Shen, *Chin. Phys. B* **24**, 127504 (2015).
5. L. Tian, B. Xu, H. Chen, Z. Mo, Z. Li, G. Liu, and J. Shen, *Sci. China Mater.* **66**, 3984 (2023).
6. M. Oboz and E. Talik, *J. Alloys Compd.* **509**, 5441 (2011).
7. N. K. Singh, K. G. Suresh, R. Nirmala, A. K. Nigman, and S. K. Malik, *J. Appl. Phys.* **101**, 093904 (2007).
8. R. L. Gao, C. L. Fu, L. Cui, Q. Y. Dong, W. Cai, Y. Zhang, X. L. Deng, Z. Y. Xu, and G. Chen, *Physica B* **457**, 36 (2015).
9. L. Cui, L. C. Wang, Q. Y. Dong, F. H. Liu, Z. J. Mo, Y. Zhang, E. Niu, Z. Y. Xu, F. X. Hu, J. R. Sun, and B. G. Shen, *J. Alloys Compd.* **622**, 24 (2015).
10. S. Gupta, R. Rawat, and K. G. Suresh, *Appl. Phys. Lett.* **105**, 012403 (2014).
11. Yu. V. Knyazev, A. V. Lukoyanov, Yu. I. Kuz'min, S. Gupta, K. G. Suresh, *JETP* **123**, 638 (2016).
12. S. Gupta, K. G. Suresh, A. V. Lukoyanov, Y. V. Knyazev, and Y. I. Kuz'min, *J. Alloys Compd.* **650**, 542 (2015).
13. H. Zhang, Y. Y. Wu, Y. Long, Y. V. Knyazev, and Y. I. Kuz'min, *J. Appl. Phys.* **116**, 213902 (2014).

14. Y. X. Wang, H. Zhang, M. L. Wu, K. Tao, Y. W. Li, T. Yan, K. W. Long, T. Long, Z. Pang, and Y. Long, *Chin. Phys. B* **25**, 127104 (2016).
15. E. D. Baglasov and A. V. Lukoyanov, *Symmetry* **11**, 737 (2019).
16. S. P. Platonov, A. G. Kuchin, R. D. Mukhachev, A. V. Lukoyanov, A. S. Volegov, V. S. Gaviko, and M. Yu. Yakovleva, *Intermetallics* **158**, 107894 (2023).
17. Z. J. Mo, J. Shen, L. Q. Yan, C. C. Tang, X. N. He, X. Zheng, J. F. Wu, J. R. Sun, and B. G. Shen, *J. Magn. Magn. Mater.* **354**, 49 (2014).
18. H. Zhang, Z. Y. Xu, X. Q. Zheng, J. Shen, F. X. Hu, J. R. Sun, and B. G. Shen, *Solid State Commun.* **152**, 1734 (2012).
19. A. G. Kuchin, S. P. Platonov, R. D. Mukhachev, A. V. Lukoyanov, A. S. Volegov, V. S. Gaviko, and M. Yu. Yakovleva, *Phys. Chem. Chem. Phys.* **25**, 15508 (2023).
20. R. D. Mukhachev and A. V. Lukoyanov, *Metals* **11**, 1296 (2021).
21. G. Yao, G. Zeng, Q. Wang, and W. Cui, *J. Magn. Magn. Mater.* **585**, 170918 (2023).
22. P. Giannozzi, O. Andreussi, T. Brumme et al. (Collaboration), *J. Phys. Condens. Matter* **29**, 465901 (2017).
23. P. Giannozzi, S. Baroni, N. Bonini et al. (Collaboration), *J. Phys. Condens. Matter* **21**, 395502 (2009).
24. J. P. Perdew, K. Burke, and M. Ernzerhof, *Phys. Rev. Lett.* **77**, 3865 (1996).
25. M. Topsakal and R. Wentzcovitch, *Comput. Mater. Sci.* **95**, 263 (2014).
26. Quantum ESPRESSO, table of pseudopotentials <https://www.quantum-espresso.org/pseudopotentials/>.
27. A. V. Morozkin, A. V. Knotko, V. O. Yapaskurt, P. Manfrinetti, M. Pani, A. Provino, R. Nirmala, S. Quezado, and S. K. Malik, *J. Solid State Chem.* **235**, 58 (2016).
28. D. J. Garcia, V. Vildosola, and P. S. Cornaglia, *J. Phys.: Condens. Matter* **32**, 285803 (2020).
29. P. Włodarczyk, L. Hawelek, P. Zackiewicz, T. Rebeda Roy, A. Chrobak, M. Kaminska, A. Kolano-Burian, and J. Szade, *Mater. Chem. Phys.* **162**, 273 (2015).
30. B. Ensign, R. Choudhary, H. Ucar, and D. Paudyal, *J. Magn. Magn. Mater.* **509**, 166882 (2020).
31. K. Yano, T. Ohta, and K. Sato, *J. Phys. Chem. Solids* **104**, 13 (2017).
32. C. Y. Lin, J. L. Li, Y. H. Hsieh, K. L. Ou, B. A. Jones, *Phys. Rev. X* **2**, 021012 (2012).
33. A. T. Hindmarch and B. J. Hickey, *Phys. Rev. Lett.* **91**, 116601 (2003).

Publisher's Note. Pleiades Publishing remains neutral with regard to jurisdictional claims in published maps and institutional affiliations.